CHALMERS
UNIVERSITY OF TECHNOLOGY

Characterization of Lipopolysaccharide -containing supported lipid bilayers

A sensing platform mimicking bacterial surfaces

Master's thesis in Biomedical engineering

PER BÖRJESSON

Department of Physics
CHALMERS UNIVERSITY OF TECHNOLOGY
Gothenburg, Sweden 2016

Master's thesis 2016:NN

Characterization of Lipopolysaccharide-containing supported lipid bilayers

A sensing platform mimicking bacterial surfaces

PER BÖRJESSON

CHALMERS
UNIVERSITY OF TECHNOLOGY

Department of Physics
Division of Biological Physics
Chalmers University of Technology
Gothenburg, Sweden 2016

Characterization of Lipopolysaccharide-containing supported lipid bilayers
A sensing platform mimicking bacterial surfaces
PER BÖRJESSON

Supervisor: Marta Bally, Department of Physics, Chalmers
Examiner: Marta Bally, Department of Physics, Chalmers

Master's Thesis 2016:NN
Department of Physics
Division of Biological Physics
Chalmers University of Technology
SE-412 96 Gothenburg
Telephone +46 31 772 1000

Cover: A graphical illustration of a bacterial surface. Aquired from: `https://tuebingen.mpg.de/uploads/RTEmagicP_YadA_Gamma_new_02.jpg`

Typeset in LaTeX
Printed by [Name of printing company]
Gothenburg, Sweden 2015

Characterization of Lipopolysaccharide containing supported lipid bilayers
A sensing platform for mimicking bacterial surfaces
PER BÖRJESSON
Department of Biological physics
Chalmers University of Technology

Abstract

Bacteria have played a huge role over the course of human history. Some bacterial strains have wrought havoc and others have proved hugely beneficial and exist in a symbiotic relationship with humans. Regardless of the type of bacteria, a better understanding of how they communicate and interact with their environment is of great value, for example when developing new types of drugs targeting bacteria. However, the complexity of bacterial membranes and the myriad of surface active molecules and proteins found on it, makes the analysis of specific biomolecular interactions occurring at bacterial membranes a challenging task. This project has therefore focused on developing sensing platforms. The first sensing platform mimics bacterial surfaces by presenting specific biomolecules in a native but well-controlled manner. It therefore comes in the form of a supported lipid bilayer (SLB) consisting of mainly 1-palmitoyl-2-oleoyl-sn-glycero-3-phosphocholine (POPC) and lipopolysaccharides (LPS). The second approach used in this thesis was to extract native membranes directly from bacteria and use these to form an SLB. The SLBs were characterized in order to verify their composition, as well as to determine their physiochemical properties and biological activity. The potential platform was also demonstrated in binding experiments using the LPS-binding molecule human lactoferrin. The outcome was analyzed using quartz crystal microbalance with dissipation monitoring (QCM-D) or total internal reflection microscopy (TIRFM). It was determined that LPS have successfully been incorporated into the SLB and that vesicles created using native membranes extracted from bacteria could also be used to form SLBs. It was also determined that these sensing platforms could be used to study a variety of biomolecular interactions involving LPS.

Keywords: lipopolysaccharide, bacteria, mimic, interaction, native membranes, QCM-D, TIRFM.

Acknowledgements

I would like to thank my supervisor Marta Bally who has given me a lot of guidance throughout the project and always took time to answer my questions. I also want to thank our collaborators from Niklas Arnbergs group in Umeås university for their help throughout the project.
Special thanks to the entire biological physics group in Chalmers for all the help they've provided and for the fun times I've had during the "fika"-breaks.
Lastly, thanks to my friends and family who have put up with me throughout my studies!

Per Börjesson, Gothenburg, Juni 2016

Contents

1
Introduction

Bacteria have throughout history had a huge impact on mankind. Regardless of whether they act as malevolent organisms or whether they are beneficial to us, a deeper understanding of how bacteria act and work could be of great use. One important aspect of bacteria is their ability to interact with their environment, a process that is mainly mediated by their surface. The surface of bacteria contains several proteins and other macromolecules that are able to interact with extracellular components. The surface of bacteria also contains molecules that are the target of many anti-bacterial compounds. Lipopolysaccharides (LPS), for example, are targeted by the antibacterial protein human lactoferrin (hLf). This protein, causes the bacterial surface to become porous making it more susceptible to other anti-microbial agents [1]. Another interesting interaction to be investigated is that between enteric virus and LPS. It has recently been hypothesized that enteric bacterial LPS favors viral infection from poliovirus occurring in the gastrointestinal tract, a process mediated by interaction with capsid molecules [2]. This raises the question of whether other enteric viruses, such as for example adenovirus 40 (AdV40) a major causative agent of viral gastroenteritis worldwide [3], also interact with LPS in a similar fashion.

In order to study interactions occuring at bacterial surfaces such as the ones mentioned above, it is of interest to develop models of the bacterial surface and to make them compatible with surface-sensing techniques that can be used to study biomolecular interactions. One promising approach for such a model is the creation of supported lipid bilayers (SLB), bilayers of lipids resting on a surface, containing bacterial surface molecules, such as LPS, as demonstrated in a recent article [4]. Alternatively surfaces that more closely resembles the bacteria have been created. One such example is a model preserving the asymmetric structure of the bacterial wall. In this model, the outer membrane rests on a thin sheet of water, mimicking the periplasm, while LPS are also incorporated in the surface [5].These examples illustrate the possibility of creating SLBs capable of mimicking the bacterial surface to different degrees.

In this project, the focus lies in trying to create SLBs of various complexities with incorporated LPS, and use these to investigate interaction with hLf and AdV40 using surface sensitive techniques.

2
Biological background

Some of the biological entities and phenomenons mentioned during the course of this report might require further explanation, this will be found here.

2.1 Human lactoferrin

Human lactoferrin is a protein of mammalian origin that is an essential part of the innate immune response. It displays several anti-bacterial effects, one being related to its ability to take up ferric irons from the environment. Bacterial growth is dependent on the presence of ferric iron, and a local depletion around the bacteria will indirectly hinder the further spread of bacterial infections. Another mode by which the hLf has been observed to help the immune system combat bacteria is by direct interaction with structural components on the bacterial surface. LPS is one structural component that has been pointed out as the target of hLf. The hLf is theorized to interact with the lipid A part of the LPS, which it oxidizes. The oxidization is a part of a number of complex steps that results in the displacement of the LPS and by extension in the destabilization of the bacterial surface. The destabilized surface will then have impaired ability to transport essential electrolytes and will also be more susceptible to other immunological agents [1].

2.2 Enteric virus and LPS

Recent papers have started investigating the effects of LPS on enteric virus. One paper looked at mice infected with orally administered poliovirus. This study reveals that mice are much less prone to infection if treated with antibiotics, which removes the gut bacteria prior to infection, leading to the hypothesis that LPS play a key role in promoting infectivity [2]. This hypothesis was then confirmed in a later paper [6], revealing that, in the presence of LPS, poliovirus displays an increased infectivity as well as an increased tolerance to temperature and pH environments that would otherwise destroy it. By exposing various mutants to LPS, it was further observed that the beneficial effect disappeared if one of the proteins located on the poliovirus surface contained a mutation, suggesting that the protein might be essential in the LPS-virus interaction [6].

2.2.1 Adenovirus type 40

There are over 50 different types of adenovirus which cause a wide array of different symptoms. What all adenovirus have in common is that they are all non-enveloped viruses with an icosahedral capsid that contains several protruding glycoproteins mediating interactions with host cells, see figure 2.1. Adenovirus type 40 is the virus investigated in this thesis. The AdV40 is an enteric virus that cause acute gastroenteritis mostly in children, although it may also infect adults. It is the third most common cause of infantile gastroenteritis after rotavirus and norovirus [3].

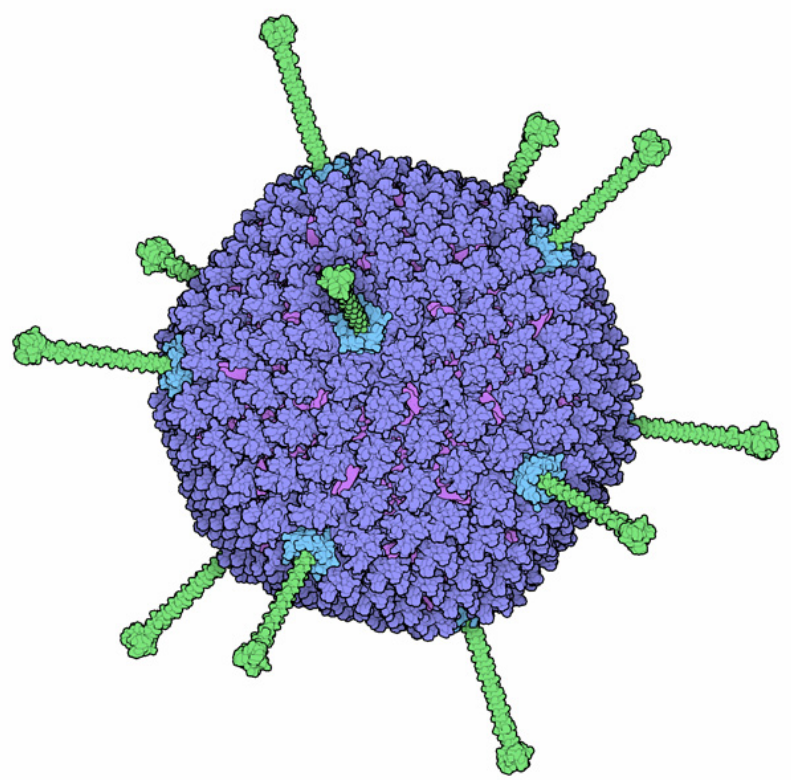

Figure 2.1: A graphical illustration of a adenovirus. The capsid is seen in purple and the protruding glycoproteins are seen in green. Image taken from [7]

3

Theory

This chapter will provide a brief explanation of the relevant techniques and principles that the project relies on.

3.1 Quartz Crystal Microbalance with Dissipation Monitoring

Quartz Crystal Microbalance with Dissipation Monitoring (QCM-D) is a technique that relies on the piezoelectric properties of the quartz crystal. A piezoelectric material is a material that can expand or contract as a response to being subjected to an electric field, see figure 3.1. In the case of the QCM-D, the electric field over the quartz crystal is alternating, causing the crystal to oscillate. Using the electric field, the QCM-D finds the fundamental resonance frequency of the crystal, which is essential for the application [8]. The fundamental frequency is expressed as follows:

$$f_0 = \frac{v_q}{2t_q} \tag{3.1}$$

Where f_0 is the fundamental resonance frequency, v_q is the speed of sound in quartz, and t_q is the thickness of the quartz crystal [9]. As can be seen, the fundamental frequency is dependent on the thickness of the quartz crystal. Now, imagine molecules adhering to the surface of the quartz crystal to form a thin film, also make the following assumptions regarding the film:

1. The molecules in the film are evenly distributed on the surface of the crystal.
2. The molecules in the film are attached firmly to the surface, and the molecules themselves are very rigid.
3. The total weight of the attached molecules are relatively small in comparison to the crystal.

With these assumptions it is possible to use the expression for the fundamental frequency in order to derive an equation that relates a change in resonance frequencies in the crystal to the amount of adsorbed mass on the surface of the crystal [8]. The German scientist Günter Sauerbrey did this and derived the Sauerbrey equation [9]:

$$\Delta f = \frac{-2nf_0^2}{\rho_q v_q}\Delta m \tag{3.2}$$

Where Δf is the change in resonance frequency, n denotes the number of the harmonic, ρ_q is the density of the quartz crystal, and Δm is the change in mass per area unit. This equation works well when approximating the weight of adsorbed

molecules in vacuum or in air, but less so when trying to investigate molecules adsorbing in a liquid medium. Indeed, the liquid medium exercises viscous and elastic effects on the surface of the crystal which violates the assumption that adsorbed molecules should be very rigid. In order to address this problem, the dissipation monitoring was introduced. The dissipation monitoring allows for observation of the viscoelastic properties of a film adsorbed to the surface of the quartz crystal. This is based on the fact that when the oscillating force is turned off, see figure 3.1 (c), the quartz crystal slowly ceases to oscillate. The rate of the oscillatory decay is dependent on how much of the energy stored in the quartz crystal can be taken up by the surrounding environment. In other words, a rigid surface will transfer only a small amount of energy during each oscillatory cycle, resulting in a low dissipation. A viscoelastic surface, on the other hand, will transfer a lot of energy to the environment in one oscillatory cycle, resulting in a higher dissipation.

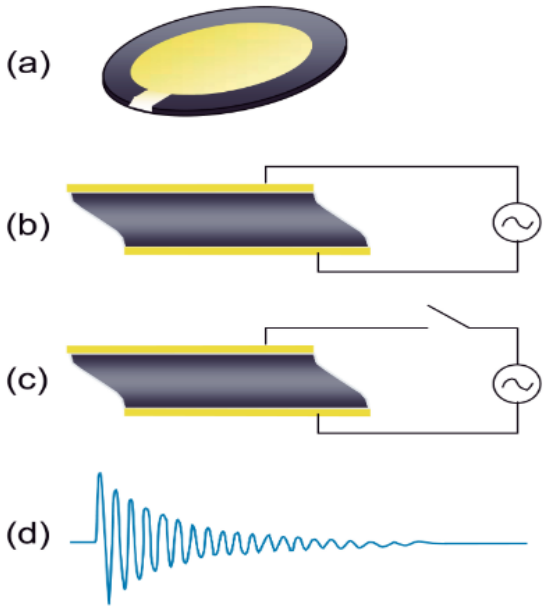

Figure 3.1: A visual representation of a QCM-D crystal and its usage. (a) A typical crystal used in a QCM-D machine. (b) The crystal starts to oscillate when subjected to an alternating electric field. (c) The electric field is turned of in order to monitor the dissipation of the crystal. (d) A typical curve depicting the decaying amplitude of the crystal, allowing for extraction of the dissipation value [8].

The dissipation constant is defined as follows:

$$D = \frac{E_D}{2\pi E_S} \tag{3.3}$$

Where D is the dissipation constant, E_D is the energy lost to the environment in one oscillatory cycle, and E_S is the energy stored in oscillating system. This definition gives a good insight regarding what is actually meant by dissipation, but it is not as helpful when trying to determine the value of D for a certain system. In order to derive the dissipation constant for a certain system using experimental data the

following expression is used:

$$D = \frac{2}{\omega\tau} \tag{3.4}$$

Where ω is the angular frequency of the oscillating system, and τ is the decay time of the crystal oscillation. The decay time is defined as the time it takes the maximum amplitude of the decaying oscillatory system to reach $1/e \times originalvalue$. In order to obtain the values for ω and τ a graphical representation of a decaying oscillatory system, such as the one seen in figure 3.1 (d), is fitted to the equation [10]:

$$A = A_0 e^{-t/\tau} sin(2\omega t + \alpha) \tag{3.5}$$

Where A is the amplitude of the system at a given time t, A_0 is the original amplitude of the system and α is the phase shift.

3.2 Surface Plasmon Resonance

Surface Plasmon Resonance (SPR) is a technique that takes advantage of surface plasmons to analyze a surface. A surface plasmon is a surface charge density wave at a metal surface which is usually created via the excitation of free electrons by exposure to light under specific conditions. One can express a dispersion relation for such a surface plasmon wave in the following, simplified, way [11]:

$$k_{sp} = \frac{\omega}{c}\sqrt{\epsilon} \tag{3.6}$$

Where k_{sp} is the plasmon wave vector, ω the angular frequency, c the speed of light, and ϵ the dielectric constant of the medium surrounding the metal surface. Now, imagine a light shining on the metal surface with the ability to excite the free electrons in the metal. The dipersion relation of the light wave vector parallel to the surface plasmon would then be expressed as:

$$k_x = \frac{\omega}{c}\sqrt{\epsilon} sin\Theta \tag{3.7}$$

Where k_x is the light wave vector parallel to the surface plasmon, and Θ is the angle at which the light hits the surface. It is key that the incident light hitting the surface at angle Ω undergoes total internal reflection in order for the reflected light to be detected. One is now able to track the amount of light lost to the surface plasmon under different circumstances. However, the most interesting part to track is the surface plasmon resonance, that is, the angle where the maximum amount of light is absorbed by the surface electrons. This angle can be solved for by solving:

$$k_{sp} = k_x \rightarrow \frac{\omega}{c}\sqrt{\epsilon} = \frac{\omega}{c}\sqrt{\epsilon} sin\Theta \tag{3.8}$$

Which cannot be practically solved. But by noting that $\sqrt{\epsilon} = n$ which is the refractive index of the medium surrounding the metal one can solve the issue by adding a material with a high refracting index to one side of the metal which the incident light can travel through. A common material to us is a glass prism. This changes the above equation to:

$$k_{sp} = k_x \rightarrow \frac{\omega}{c} n = \frac{\omega}{c} n_g sin\Theta \tag{3.9}$$

Where $n_g > n$, making it possible to solve for Θ by noting that:

$$\Theta = arcsin(\frac{n}{n_g}) \tag{3.10}$$

Now, the refractive index n for the non-glass medium can be changed as molecules adsorb to the surface of the metal, thus changing the angle at which surface plasmon resonance occurs. This allows for effective tracking of molecule-surface interaction [11].

3.2.1 Dual wavelength SPR

The SPR tracks the angle at which the plasmon resonacne occurs, which from now on will be denoted as R. The SPR responce can also be expressed as:

$$R = \frac{S\frac{dn}{dC}\varphi}{\delta} \tag{3.11}$$

Where S in the sensitivity factor, $\frac{dn}{dC}$ is a change in refractive index with respect to molecule concentration in bulk, φ is a dimensionless factor, and δ is the decay length of the SPR evanescent field. The dimensionless factor, φ, can in turn be expressed in the following way:

$$\varphi = (1 - e^{-d/\delta})\frac{\delta}{d} \tag{3.12}$$

Where d is the thickness of surface adhered molecules/layers. The thickness can be a bit tricky to determine from the above equation alone, but it is possible to determine d directly from using a ratio between the response for two different wavelength, i.e the following equation:

$$\frac{R_{\lambda_1}}{R_{\lambda_2}} = \frac{S_{\lambda_1}\frac{dn}{dC}_{\lambda_1}\varphi_{\lambda_1}\delta_{\lambda_2}}{S_{\lambda_2}\frac{dn}{dC}_{\lambda_2}\varphi_{\lambda_2}\delta_{\lambda_1}} \tag{3.13}$$

The determination of thickness d from this equation is dependent on all other factors beeing known, as well as the condition $d << \delta$ being true.

3.3 Total Internal Reflection Fluorescence Microscopy

Total Internal Reflection Fluorescence Microscopy (TIRFM), is a technique developed with the purpose of investigating events taking place on surfaces and it is typically used to investigate the interactions or movements of biomolecules at different interfaces. The principle by which the TIRFM operates is as follows: An excitation beam travels at a high angle relative to a glass slide which acts as a sensing interface. The excitation beam must travel in an angle higher than a critical angle so that when the beam hits the surface it will be completely internally reflected, i.e. the beam cannot be allowed to refract into the sample [12]. Once this

total internal reflection occurs, a very thin electrical field will be created, called the evanescent field, see figure 3.2.

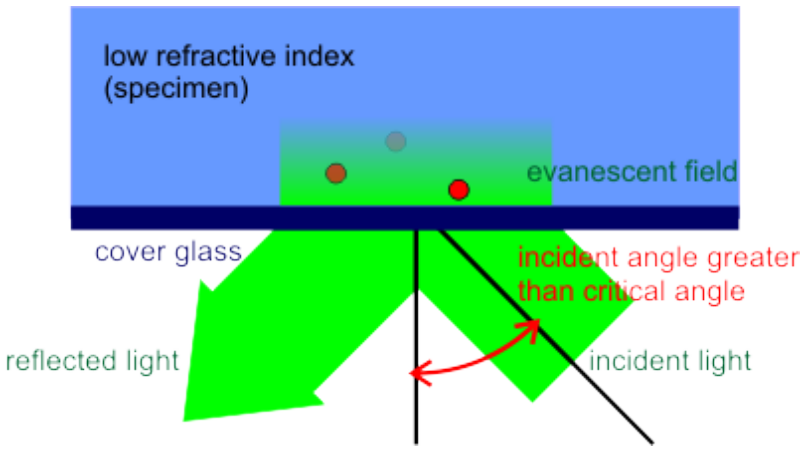

Figure 3.2: In TIRFM, an incident light beam is totally reflected by a surface, creating an evanescent field. The evanescent field can in turn excite fluorophore markers placed on the sample surface being investigated. [13].

This evanescent field can be used to excite fluorophores located close to the surface of interest. As the fluorophores are excited they give of light which in turn can be detected by the microscope, allowing for the detection of, for example, fluorescently marked biological species. One of the key concepts of the TIRFM is the exponentially decaying intensity of the evanescent field with distance from the surface. This exponential decay hinders potential fluorophores in the bulk liquid from getting activated, allowing for the direct observation of the fluorescent surface with reduced background noise from the bulk molecules [12].
It is, however, possible to alter the penetrating depth of the evanescent field in order to be able to observe events occurring at different levels in close vicinity to the surface. To understand how this is possible, a mathematical model of the physical system will be explained. Imagine a beam of light propagating through a medium of high refractive index (such as glass) only to reach a flat surface connected to medium of relative low refractive index (such as water in the bulk). The critical angle which the incident beam of light needs to exceed in order to undergo total reflection is expressed as:

$$\Theta_c = sin^{-1}(\frac{n_b}{n_g}) \tag{3.14}$$

Where Θ_c is the critical angle, n_b is the refractive index of the bulk, and n_g is the refractive index of the glass. Should the incident angle exceed the critical angle, an evanescent field will appear around the point of reflection. This electrical field will have a intensity, I, which decays when traveling away from the surface in the z direction as follows:

$$I(z) = I_0 e^{-z/d} \tag{3.15}$$

where

$$d = \frac{\lambda_0}{4\pi}(n_g^2 sin^2\Theta - n_b^2)^{-1/2} \tag{3.16}$$

and λ_0 is the wavelength of the incident light beam in vacuum. As can be seen, the intensity gradient of the evanescent field can be altered by altering the incident angle Θ. In other words, decreasing the incident angle increases the thickness of the evanescent field, as long as the condition $\Theta \geq \Theta_c$ is fulfilled [12].

3.3.1 Fluorescent Recovery After Photobleaching

Fluorescent Recovery After Photobleaching (FRAP) is a technique that allows for the study of the mobility of cellular components. The main principle is that a fluorescent area is bleached, usually via laser illumination, and the fluorescent molecules outside the bleached area are allowed to diffuse into the bleached region of interest (ROI). This fluorescent recovery is observed throughout the process, allowing for determination of the diffusivity of the fluorescent molecules. The recovery data also gives information regarding any immobile fraction of the bleached molecules [14]. An example of this can be seen in figure 3.3.

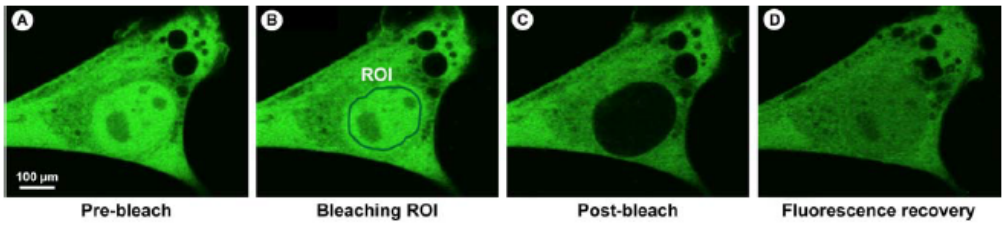

Figure 3.3: The FRAP process: A) A cell with fluorescently marked molecules prior to photobleaching. B) Region Of Interest to be bleached is outlined. C) Fluorescent bleaching is performed, leaving the ROI as a dark spot. D) Fluorescent molecules migrate into the bleached spot. [14].

It is, as mentioned, possible to determine the diffusion coefficient for fluorescent molecules by using FRAP. This is, however, not trivial. For a two dimensional surface consisting of fluorescent molecules the diffusion coefficient can be approximated after photobleaching by, for example, using the Soumpasis equation [15]:

$$D_{r_n} = 0.224\frac{r_n^2}{\tau_{1/2}} \tag{3.17}$$

Where D_{r_n} is the diffusion coefficient, r_n is the radius of a uniform bleached spot in the two dimensional surface, $\tau_{1/2}$ is the half time of recovery, and the constant 0.224 is a numerically determined constant. In order to use the Soumpasis equation, one has to determine $\tau_{1/2}$, which can be done by tracking the fluorescent intensity of the bleached spot with regards to time. The intensity is then subjected to non-linear curve fitting with the following equation [14]:

$$I_t = M_f\left(1 - e^{-\tau t}\right) \tag{3.18}$$

Where I_t is the fraction of the original intensity before photobleaching, I_0, at time t, M_f is the combined intensity of the mobile fraction of fluorescent molecules, and τ is a constant related to the recovery of the photobleached spot. By looking at equation 3.18, one can see that as $t \to \infty$, then $I_t \to M_f$. As a consequence it is possible to determine the half time by substituting I_t with $\frac{M_f}{2}$ and solve for t. This gives the equation:

$$\tau_{1/2} = \frac{ln(0.5)}{-\tau} \tag{3.19}$$

Which can be used in equation 3.17 to determine the diffusion coefficient.
The immobile fraction, γ_0, can also be of interest when trying to characterize a surface, and is defined as:

$$\gamma_0 = 1 - M_f \tag{3.20}$$

The intensity profile after photobleaching is illustrated in figure 3.4

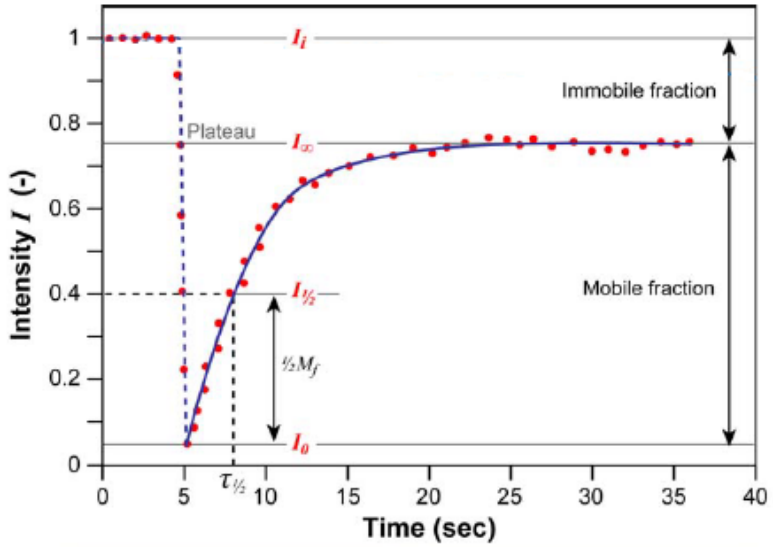

Figure 3.4: Illustration of the intensity recovery after photobleaching. The bleaching takes place at the 5 seconds mark and final recovery is reached after approximately 25 seconds. The figure was taken from [14] and has been altered.

The approach to determine the diffusion coefficient explained in this section is quite simplified and more sophisticated methods are usually used in order to analyze data collected from FRAP such as the method developed by Peter Jönsson, explained in his paper [16].

3.4 Fluorescence Resonance Energy Transfer

Fluorescence Resonance Energy Transfer (FRET) relies on the use of fluorophore pairs. Fluorophore pairs are pairs of fluorecent molecules where one of the molecules

acts as a quencher for the other molecule, by absorbing the light emitted by the first molecule to then emit light at another wavelength, see figure 3.5.

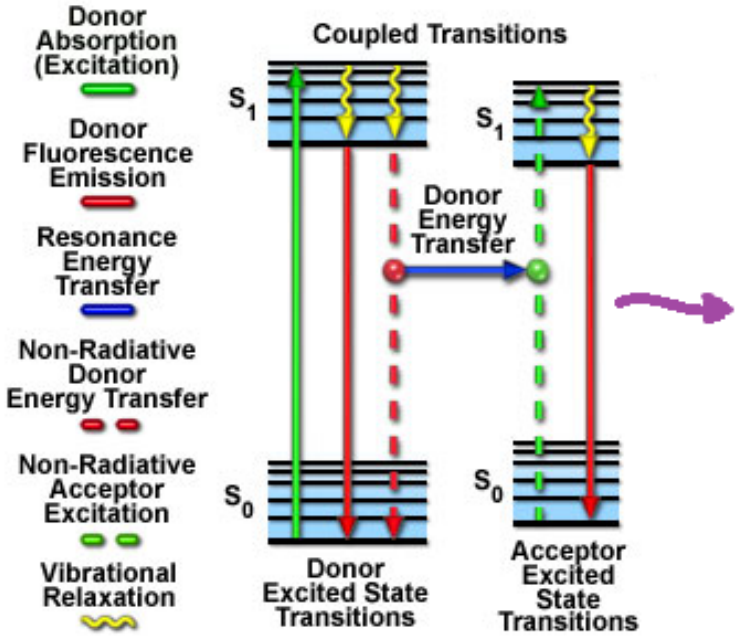

Figure 3.5: A schematic illustrating the energy transfer between fluorophore pairs. The donor molecule gets excited by incoming light and then relaxes, letting of light of a different wavelenght which can be taken up by the acceptor molecule. The acceptor molecule gets excited, and as it relaxes,emits light at a wavelength lower than the one used to excite it [17].

This property of fluorescent pairs allows for the study of fluorescently marked molecules, and their interaction or dissociation with molecules marked with the paired fluorescent tag. This phenomenon can for example be used to study where and how different proteins interact. It can also be used to study how/if different molecules separate under certain circumstances [17]. One example of when the tracking separation of molecules is useful is in the case of vesicle merging. Merging vesicles can be tracked by introducing fluorescent pairs in one type of vesicle and have vesicles of another type mixed into the same solution. Should the two types of vesicles fuse, an increased number of fluorescent pairs is separated by lipids from other vesicles and the merging of vesicles would be detectable by the FRET.

4

Materials and Methods

4.1 Vesicle preparation

Vesicles consisting of 1-palmitoyl-2-oleoyl-sn-glycero-3-phosphocholine (POPC) from Avanti Polar Lipids inc were created with incorporated biomolecules in the form of LPS/LTA. The different biomolecules incoporated into vesicles were:

- Lipopolysaccharide from Escherichia coli K12 (LPS-Ek) from InvivoGen
- Lipoteichoic acid from Staphylococcus aureus (LTA) from Sigma-Aldrich
- Lipopolysaccharides (rough strains) Escherichia coli J5, Rc mutant (LPS-Rc) from Sigma-Aldrich
- Lissamine^{TM} rhodamine B DHPE molecular probes from Invitrogen/ThermoFisher

Round bottom flasks were rinsed with chloroform, then about 1-2 ml chloroform was added to the flasks. POPC and LPS/LTA (stored at -20^oC in endotoxin-free water) were added to the chloroform in a desired weight ratio and dried in nitrogen flow for 30 minutes. If the vesicles were to be used in either FRAP or TIRFM expreiments, 1wt% of rhodamine lipids were also added to the chloroform. The round bottom flasks were vacuum pumped for 1.5 hours. The dried samples were then resuspended in 1 ml of buffer, which varied depending on the type of vesicle. Buffers used were:

- 10 mM M phosphate buffer 2.7 mM KCl 137 mM $NaCl$ pH 7.4 (PBS)
  Used when preparing pure POPC vesicles
- 20 mM Citric acid 150 mM $NaCl$ pH 4.8 (Citrate)
  Used when preparing LPS/LTA vesicles, buffer used for most vesicles
- 10 mM HEPES 150 mM $NaCl$ 3mM $CaCl_2$ pH 7.4 (Ca buffer)
  Used when preparing LPS/LTA vesicles

Resuspended vesicles were extruded 11 times using an extruder from Avanti Polar Lipids inc. and Whatman 30 nm membrane filters, unless the vesicles were intended for tracing, then 100 nm filters were used. The so-prepared vesicles were stored in sealed containers at 4^oC.

4.2 QCM-D experiments

The QCM-D device used was an E4 sensor system from Q-sense/Biolin scientific, and the substrates were subjected to UV ozone cleaning and were then cleaned in SDS and MQ-water before use. The QCM-D was operated at a flow speed of 50 μl/min if not stated otherwise. Before bilayer formation the QCM-D crystals were exposed to the appropriate buffer for bilayer formation in order to form a baseline.

The buffer used was dependent on which vesicles were used to form a bilayer. Vesicle stocks were diluted to 0.1 mg/ml to a total volume of 1 ml and were flown over the QCM-D crystal until SLB-formation took place. When appropriate, bilayers were subjected to a 10 minutes osmotic shock using ultrapure water from a Synergy®UV purification system from Merck Millipore.

4.2.1 Human Lactoferrin and Adenovirus

Human lactoferrin and adenovirus (type 5, 37 and 40) were kindly provided by Niklas Arnberg and Carin Årdahl from Umeå University. The Lactoferrin from human milk was procured from Sigma-Aldrich. The adenoviruses were cultivated by the Arnberg group.
Before introduction to the QCM-D, the human lactoferrin was diluted to a concentration of 0.02 mg/ml with a total volume of 500 μl using PBS. Pure PBS buffer was added to the SLB in the QCM-D before and after the addition of lactoferrin suspension.
The adenovirus were diluted in PBS to a concentration of 5.89 μg/ml up to a total volume of 2 ml before introduction to the QCM-D. Pure PBS buffer was added to the SLB in the QCM-D before and after the addition of adenovirus solution.

4.3 FRAP and TIRFM experiments

FRAP and TIRFM experiments were all performed on an inverted Nikon Eclipse Ti-E microscope from Nikon Corporation, Japan, and equipped with an Andor Ixon+ camera from Andor Technology, Ireland. The photobleaching source in the FRAP experiment was a diode pumped solid-state 532 nm laser from B&W TEK Inc. with a 100 mW output.
In both types of experiments, samples were added to PDMS wells of about 3mm in depth and width. The PDMS wells rested on a clean glass substrates, cleaned by boiling for two hours in a 7x cleaning solution from MP. For the FRAP experiments, 10 μl of fluorescently marked vesicles with a concentration of 0.3 mg/ml were added to the wells in order to form bilayers. Added samples were left to incubate for 15 minutes. FRAP was then performed after rinsing 7 times with 30 μl PBS buffer and then again after a 10 minute osmotic shock, performed by rinsing 7 times with 30 μl with deionized water. In one case FRAP was performed on the SLBs after adding 1 μl hLF with a concentration of 10 mg/ml to the wells.
For the TIRFM experiments to investigate AdV40 interaction, SLBs were formed by adding 10 μl of non-fluorescently marked vesicles with a concentration of 0.3 mg/ml to the wells. The samples were incubated for 15 minutes and then rinsed 7 times using 30 μl PBS buffer. After rinsing the well, the volume was adjusted to approximately 20μl and 5 μl adenovirus 40 solution with a concentration of 576.8 μg/ml was added to the well and left to incubate for 30 min. The wells were then rinsed again as before, using PBS buffer, and 5 μl POPC vesicles with a concentration of 4 mg/ml were added to the wells along with 10 μl fluorescently marked LPS-containing vesicles with a concentration of 0.01 mg/ml. The LPS incorporated in the bilayers were always of the same type as the LPS incorporated

into the fluorescent vesicles. Before addition of POPC and fluorescent vesicles, the wells contained about 10 μl solution. The surfaces were then observed using TIRFM.

4.4 Surface Plasmon Resonance

Vesicles of 0.05 wt% and 30 wt% LPS-Ek in POPC were prepared as previously mentioned and diluted in citrate buffer to concentrations of 0.05 mg/ml and 0.67 mg/ml respectively. Vesicle solutions were introduced to a Multi-Parametric SPR of the type SPR Navi 220A, bought from Bionavis, Finland. Samples were run through the SPR at 50 μl/min for 7 minutes and injection mode was set to parallel. Scanning wavelengths were set to 670 nm and 785 nm for both samples.

4.5 Native Membrane Vesicles

E.Coli K12 MG1655 bought from Leibniz Institute DSMZ, were cultured in LB broth media from Sigma Aldrich at 37^oC over night. The resulting bacterial culture were centrifuged using a Mikro22R centrifuge from Hettich at 3710g at 4^oC for 60 minutes. Supernatant was discarded and the pellet resuspended in PBS buffer at twice the concentration used earlier in this chapter (2xPBS), cOmplete™, EDTA-free Protease Inhibitor Cocktail from Sigma Aldrich was also added to the resuspension. Cell suspension was run through a cell crusher in order to lyse cells. The resulting solution was put in a Optima LE-8K ultracentrifuge from Beckman Coulter and the centrifuge was run at 10000g at 4^oC for 20 minutes. Supernatant was then transferred to new tubes which in turn were placed in ultracentrifuge which ran at 250000g at 4^oC for 90 minutes. Supernatant was discarded and resulting pellets were then resuspended in 2xPBS and mixed with 20% glycerol (volume). Aliquotes of NMV solutions were rapidly frozen using liquid nitrogen and stored in -80^oC.

4.5.1 Characterization of Native Membrane Vesicles

A FRET assay was performed in order to verify the ability of NMVs to merge with synthetic vesicles. FRET vesicles, extracted with a 100 nm filter, consisting of 1 mol% Rhodamine DOPE lipids 1 mol% NBD DOPE lipids and 98 mol% POPC were mixed with E.Coli NMVs in a 1:30 ratio and diluted to a concentration of about 1 mg/ml using PBS. The mixture was divided into two samples. One sample was sonicated at 37^oC for ten minutes, and the other not sonicated as a negative control. The two samples were investigated using a QM-4/2005 spectrofluorometer from Photon Technology International Inc in order to verify merging of sonicated vesicles.

In order to confirm the NMVs ability to form bilayers the PEG/POPC vesicles consisting of 3.5 wt% PEG5000-ceremide and 96.5 wt% POPC were merged with the NMVs and tracer vesicles, consisting of 1 wt% Rhodamine, 99 wt% POPC, via 10 minutes sonication at 37^oC. The ratio of NMV to PEG/POPC was varied in order to investigate the influence of NMV content on bilayer formation, ratios mixed were:

- 10% wt NMV to 90% wt PEG/POPC ,2 μl of 2 μg/ml tracer vesicles were also added, creating a total volume of 82 μl with a total vesicle concentration of about 1mg/ml.
- 20% wt NMV to 80% wt PEG/POPC ,2 μl of 2 μg/ml tracer vesicles were also added, creating a total volume of 82 μl with a total vesicle concentration of about 1mg/ml.
- 30% wt NMV to 70% wt PEG/POPC ,2 μl of 2 μg/ml tracer vesicles were also added, creating a total volume of 82 μl with a total vesicle concentration of about 1mg/ml.
- 40% wt NMV to 60% wt PEG/POPC ,2 μl of 2 μg/ml tracer vesicles were also added, creating a total volume of 82 μl with a total vesicle concentration of about 1mg/ml.

14 μl PBS was added to four seperate PDMS wells and put on the TIRF-microscope. 4 μl NMV+PEG/POPC vesicles were added to the wells, one type of NMV ratio per well, and bilayer formation was monitored.
When analysing NMV + PEG/POPC with QCM-D, similar ratios were mixed with a total vesicle concentration of 0.1 mg/ml.

5
Results

5.1 Forming and characterizing LPS bilayers

Supported lipid bilayers were formed as described in the method section, and these bilayers were characterized using both the QCM-D and FRAP methods. The QCM-D allowed for monitoring of of the bilayer formation kinetics. It also provided information regarding how the structure and mass composition of the SLB was affected when different parameters were changed, such as buffer type or amount of LPS incorporated in the vesicles.
The FRAP experiments gave information about the mobility of the lipids in the different types of SLBs. The microscope used for the FRAP experiments also allowed for a more direct view of the SLB surface structure.

5.1.1 Bilayer formation conditions

In order to create SLBs efficiently, it was important to determine the optimal buffer conditions in which to form POPC-LPS/LTA bilayers. Vesicles consisting of nothing but POPC lipids can adhere to, and form bilayers on, the hydrophilic and negative surface of the silica coated QCM-D crystals at neutral pH. The PBS buffer thus works fine for POPC vesicles. When sugars are incorporated into the vesicles, however, the negative charge of the silica surface repels the negatively charged LPS/LTA sugars, making SLB formation less energetically favorable. Several buffers were thus investigated in order to attempt the creation of SLBs from the LPS/LTA containing vesicles. Representative results using LTA-incorporated vesicles can be seen in figure 5.1.

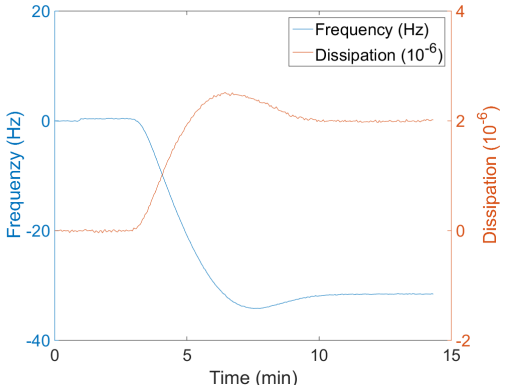

(a) Bilayer formation with LTA incorporated POPC vesicles in Citrate pH 4.8.

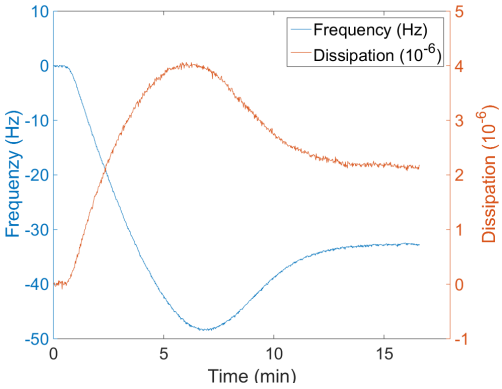

(b) Bilayer formation with LTA incorporated POPC in Ca buffer pH 7.4.

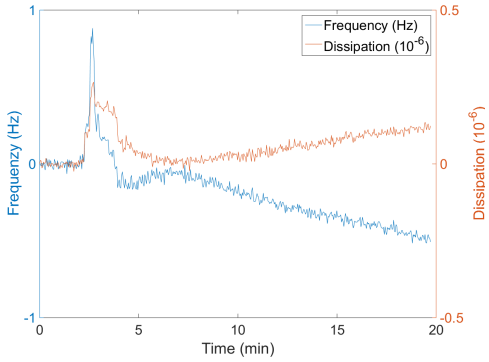

(c) Bilayer formation with LTA incorporated POPC vesicles in PBS pH 7.4.

Figure 5.1: Frequency and dissipation vs time data of a bilayer formation with LTA incorporated POPC vesicles in different buffers. PBS proved to hinder bilayer formation altogether in this instance, whereas both calcium and citrate buffer facilitated bilayer formation and gave similar final values in regards to frequency and dissipation.

An approach to be used when trying to overcome electrostatic repulsion, which is to modify the pH of the buffer. In this case a buffer with pH 4.8 will be used. A low pH will cause a higher fraction of the negative side groups present on both the crystal surface as well as on the vesicles to lose their negative charge, making the bilayer formation a more probable event. Results of this approach, using citrate buffer with pH 4.8, can be seen in figure 5.1a. As an alternative to lowering the pH, calcium ions can be used. The Ca^{2+} ions interacts with the negative charges on the silica surface and on the vesicles in a way that shields the charges from one another. This reduces the energy barrier between the negative surface and the negative vesicle, allowing for bilayer formation [18]. Figure 5.1b shows successful bilayer formation in the presence of calcium buffer. As can be seen in figure 5.1c, using PBS buffer with a pH of 7.4 results in a very low amount of vesicle absorption. The results showcased in figure 5.1b and 5.1a indicated that both calcium and citrate buffers

were viable options to form SLBs on silica surfaces with negatively charged vesicles. One drawback of the calcium buffer, however, was the need to remove the Ca^{2+} ions which could interfere with other interactions of interest on the SLB and lipid/LPS organization on the bilayer. In order to remove the ions, ethylenediaminetetraacetic acid (EDTA), which chelates Ca^{2+}, was used. However, this approach added extra steps to the procedure. It can also be noted that the stable frequency and dissipation values were very similar when comparing the bilayer formation process in the citrate and calcium buffers. Since the same trend could be observed for LPS-Ek and LPS-Rc, see Appendix 1 figure A.1 and A.2, it was decided that citrate should be used as a buffer when forming the SLBs during all experiments.

5.1.2 Formation of Supported Lipid Bilayers

SLBs of different compositions were formed on the surface of QCM-D crystals and were subsequently analyzed using the QCM-D apparatus. Figure 5.2 showcases the formation of sample bilayers of different compositions.

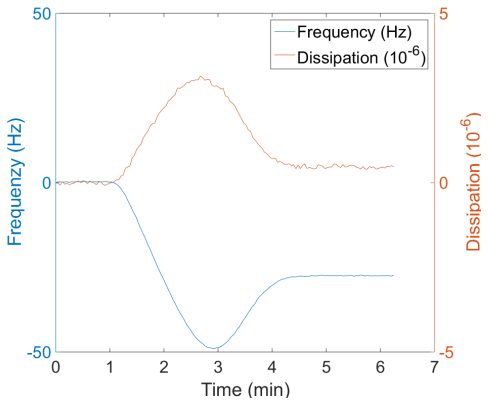

(a) Bilayer formation with POPC vesicles.

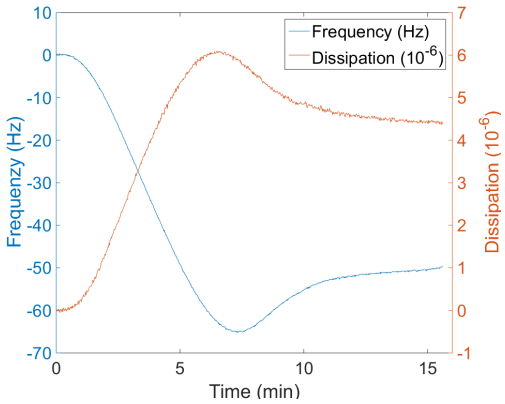

(b) Bilayer formation with POPC vesicles with incorporated LPS-RC.

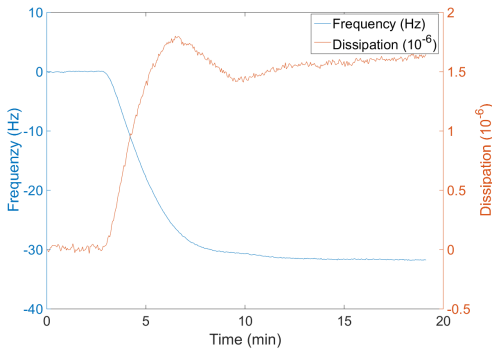

(c) Bilayer formation with POPC vesicles with incorporated LPS-ek.

Figure 5.2: Frequency and dissipation vs time data curves displaying the characteristic appearance associated with bilayer formation. The experiments shown in (a) and (c) were performed in citrate buffer and the LPS concentration was 10 wt% in both cases (b) was performed in PBS using POPC vesicles.

In figure 5.2a the characteristic curve indicating bilayer formation is clearly visible. The same goes for figure 5.2b, although the final values seen for the frequency and dissipation are more extreme than the values found in figure 5.2a, but lowers after an osmotic shock to around $-35Hz$ and $1,9 \cdot 10^{-6}$ respectively. One possible reason for this behavior could be the presence of many unruptured vesicles on the surface, and indeed, after an osmotic shock the frequency and dissipation values dropped to the more expected values listed in table 5.1, further indicating that the phenomenon was caused by unruptured vesicles.
Looking at figure 5.2c, the frequency curve differs from what one would expect from a bilayer formation in that the frequency only steadily reaches a steady value, whereas the dissipation behaves normally, with a maximum value reached shortly before decreasing into a lower steady state. The observed behaviour could be explained by surface adhered vesicles containing the LPS-Ek rupturing in parallel with new vesicles arriving at the surface which in turn rupture as they land, resulting in the absence of the frequency minimum often characterizing the SLB formation process. Attempts at forming bilayers using different LPS/LTA compositions were performed and table 5.1 showcases the different compositions used, as well as the frequency and dissipation values observed after bilayer formation.

Table 5.1: Frequency and dissipation values during different stages of the SLB formation. Δf is the steady state frequency shift observed after the bilayer formation. ΔD describe the analogous case for the dissipation. The (-) sign indicate that the sample was investigated before osmotic shock, whereas the (+) sign indicate that the sample was investigated after an osmotic shock.The simple $-$ sign indicate that no data is available. In all cases bilayer formation was carried out in citrate buffer, except for POPC where PBS was used.

SLB composition	Δf (Hz) (-)	Δf (Hz) (+)	ΔD (10^{-6}) (-)	ΔD (10^{-6}) (+)
Pure $POPC$	-25,9 $\pm 1,0$	-	0,4 $\pm 0,8$	-
$2\% LPS-Ek$	-28,8 $\pm 0,1$	-	1,4 $\pm 0,2$	-
$10\% LPS-Ek$	-29,8 $\pm 2,54$	29,5 $\pm 2,1$	1,3 $\pm 0,3$	1,5 $\pm 0,6$
$30\% LPS-Ek$	-34,5 $\pm 0,7$	-32,5 $\pm 0,7$	3,6 $\pm 0,8$	2,92 $\pm 0,53$
$10\% LPS-Rc$	-52,8 $\pm 7,6$	-35,2 $\pm 3,1$	4,9 $\pm 1,6$	1,87 $\pm 0,8$
$10\% LTA$	-31,5 $\pm 0,7$	-31,5 $\pm 0,7$	2,4 $\pm 0,5$	1,8 $\pm 0,3$

The presence of the relatively heavy LPS/LTA in the POPC bilayer would intuitively increase the frequency change detected by the QCM-D. In a similar way, the long LPS/LTA chains should alter the viscoelastic properties detected. Looking at table 5.1 one can see an indication that an increased amount of LPS-Ek in the bilayer increases the amplitude for both the frequency and the dissipation. Looking at the steady state frequency shift and dissipation shift for the $2\% LPS-Ek$ and the $30\% LPS-Ek$ this trend in quite clearly observed. This could be seen as an indirect indication that the LPS are incorporated into the bilayer. Table 5.1 also shows that the effect of osmotic shock is low, with the exception of the LPS-Rc, where a big change in both frequency and dissipation can be seen after introduction of deionized water.

In order to further confirm the presence of LPS-Ek in the bilayers, several LPS-Ek containing bilayers were formed in the QCM-D, each bilayer with a different amount of LPS-Ek Incorporated. The bilayers were formed in PBS buffer, since an increasing amount of negatively charged sugars in the vesicles would result in slower bilayer formation under the mentioned circumstances, as discussed in section 5.1.1. Figure 5.3 shows the results of this experiment.

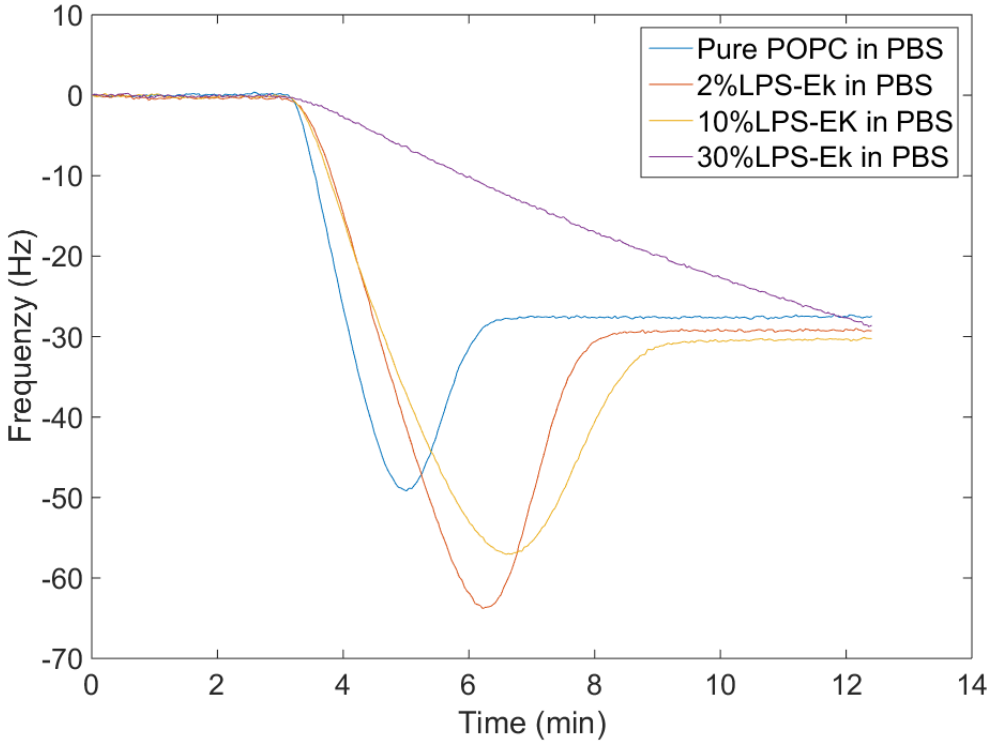

Figure 5.3: Frequency vs time data displaying the difference in bilayer formation speed for 0, 2, and 10% LPS-EK incorporated in POPC vesicles. The attempt at forming a bilayer with 30% LPS-Ek is also included. The bilayers were formed in PBS buffer.

The results displayed in figure 5.3 confirm that at increased LPS-Ek concentrations bilayer formation is less favorable with slower kinetics. For the highest LPS content, no bilayer formation was observed within the time of the experiment. This strongly suggests that LPS-Ek has been incorporated in the vesicles in a concentration dependent manner. An analogous indication of the presence of LTA in the vesicles can be seen in figure 5.1 where the precence of LTA greatly inhibits vesicle formation in the precense of PBS.
The data presented in this section indicates that bilayer formation took place for all tested vesicle compositions. Questions were raised, however, when observing results such as those presented in figure 5.2b and 5.2c, on whether the higher steady state frequency and dissipation values relative to figure 5.2a are due to the presence of LPS in the bilayers or if the differences are due to an increased presence of unruptured vesicles. In order to further investigate this, FRAP experiments were performed.

5.1.3 Characterisation of Supported Lipid Bilayers using FRAP

SLBs of different LPS/LTA compositions were formed as described in chapter 4. The formed SLBs were then photobleached and the fluorescence recovery was recorded and used to derive diffusion coefficients as well as immobile fractions for the separate samples. In order to further investigate the effect of water shock on the formed bilayers, FRAP was performed on the SLBs both before and after the water shock was applied. The recorded data is summarized in table 5.2

Table 5.2: Diffusion coefficients, D, for the different types of SLBs. The immobile fraction, γ_0, is also listed. All FRAPs were performed in PBS. The (-) sign indicates that the sample was investigated before osmotic shock, whereas the (+) sign indicates that the sample was investigated after an osmotic shock. The simple $-$ sign indicate that no data is available.

SLB composition	D ($\mu m^2/s$) (-)	D ($\mu m^2/s$) (+)	γ_0 (-)	γ_0 (+)
POPC	1,70 $\pm 0,11$	1,6 $\pm 0,07$	0,01 $\pm 0,01$	0,01 $\pm 0,01$
$2\%LPS-Ek$	1,51 $\pm 0,02$	1,51 $\pm 1,14$	0,00 $\pm 0,01$	-0,02 $\pm 0,02$
$10\%LPS-Ek$	1,96 $\pm 0,10$	1,85 $\pm 0,08$	0,01 $\pm 0,01$	0,01 $\pm 0,01$
$30\%LPS-Ek$	1,15 $\pm 0,10$	1,29 $\pm 0,11$	0,01 $\pm 0,05$	0,02 $\pm 0,02$
$10\%LTA$	-	1,43 $\pm 0,18$	-	0,01 $\pm 0,01$
$10\%LPS-Rc$	1,48 $\pm 0,06$	1,69 $\pm 0,24$	0,01 $\pm 0,03$	0,03 $\pm 0,04$
$10\%LPS-Rc$ + hLf	-	1,71 $\pm 0,07$	-	0,04 $\pm 0,02$

Looking at table 5.2, one can observe that the immobile fraction is in all cases below 4%, which indicates that almost all vesicles have ruptured since non-ruptured vesicles would result in an immobile fraction as their lipids do not recover. The high amount of ruptured vesicles also support the claim made in section 5.1.2 that the higher frequency and dissipation values seen in table 5.1 were due to the long and heavy LPSs present in the SLBs and not to unruptured vesicles. Looking at the diffusion coefficients listed in table 5.2, it is difficult to see any clear trends connected to the amount of incorporated LPS in the SLB. The SLBs containing 30% LPS-EK clearly have lower diffusion coefficients associated with them than the SLBs containing less LPS-Ek. However, the 10% LPS-Ek has a higher diffusion coefficient than the rest of the samples. It could be that different amounts of LPS-Ek incorporated in the bilayers give rise to different conformations of the LPS-Ek on the surface it is expressed. Such a phenomenon could give the surface slightly different properties unique for specific concentrations of LPS-Ek. Such a phenomenon could also explain the results regarding dissipation seen in table 5.1, where the 10% LPS-Ek again does not follow the trend of increasing dissipation with increasing LPS-Ek content.
The water shock did not significantly affect the diffusion coefficient and immobile fraction of most bilayers, with exception of LPS-Rc where a small difference might be seen. This corresponds well with the data seen in table 5.1, further indicating a higher amount of unruptured vesicles in absence of osmotic shock for this specific composition.

5.1.4 Characterization of Supported Lipid Bilayers using SPR

Dual wavelength SPR was used in order to get an indication regarding the thickness of some of the bilayers. Bilayers containing LPS-Ek 0.05 and 30% were formed in the SPR and the process was monitored, yielding figure 5.4.

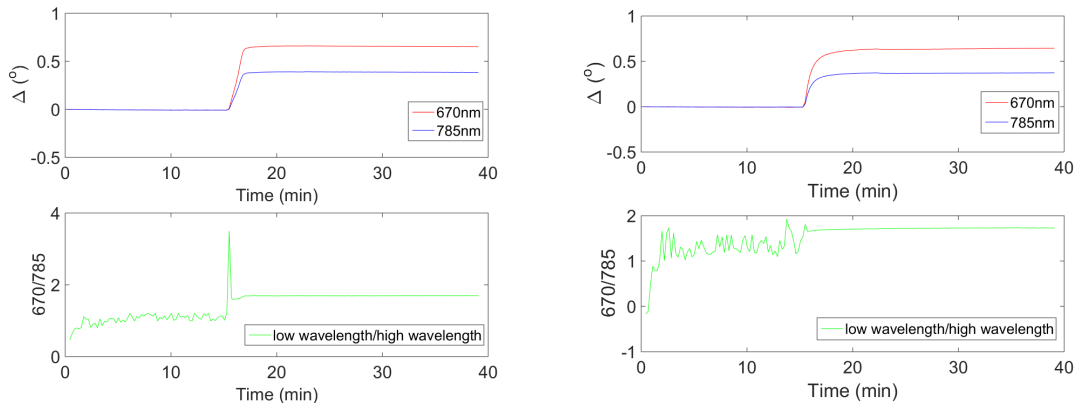

(a) **(b)**

Figure 5.4: Results from dual wavelength SPR using 670 and 785 nm light. (a) shows the formation of the 0.05% LPS-Ek bilayer as well as the ratio between the SPR response of the two wavelengths. (b) shows the analogous case of the 30% LPS-Ek

The topmost part of figure 5.4 show that vesicles start adhering to the surface slightly after the 15 minute mark. Shortly thereafter a steady state is reached for both wavelengths, indicating that no more material is adhering to the surface. The lower part of figure 5.4, showing the ratio of the signal measured at both wavelengths, both end up at a steady state very close to 1.7, which according to [19] (not yet published) indicate that the thickness of the adhered material, the bilayers, is slightly below 5nm.

5.2 Characterizing E.Coli Native Membrane Vesicles

NMVs were created as described in chapter 4 and were investigated with a FRET assay in order to confirm their ability to fuse with synthetic POPC/PEG vesicles and hence to form hybrid vesicles. The result from the FRET assay can be seen in figure 5.5.

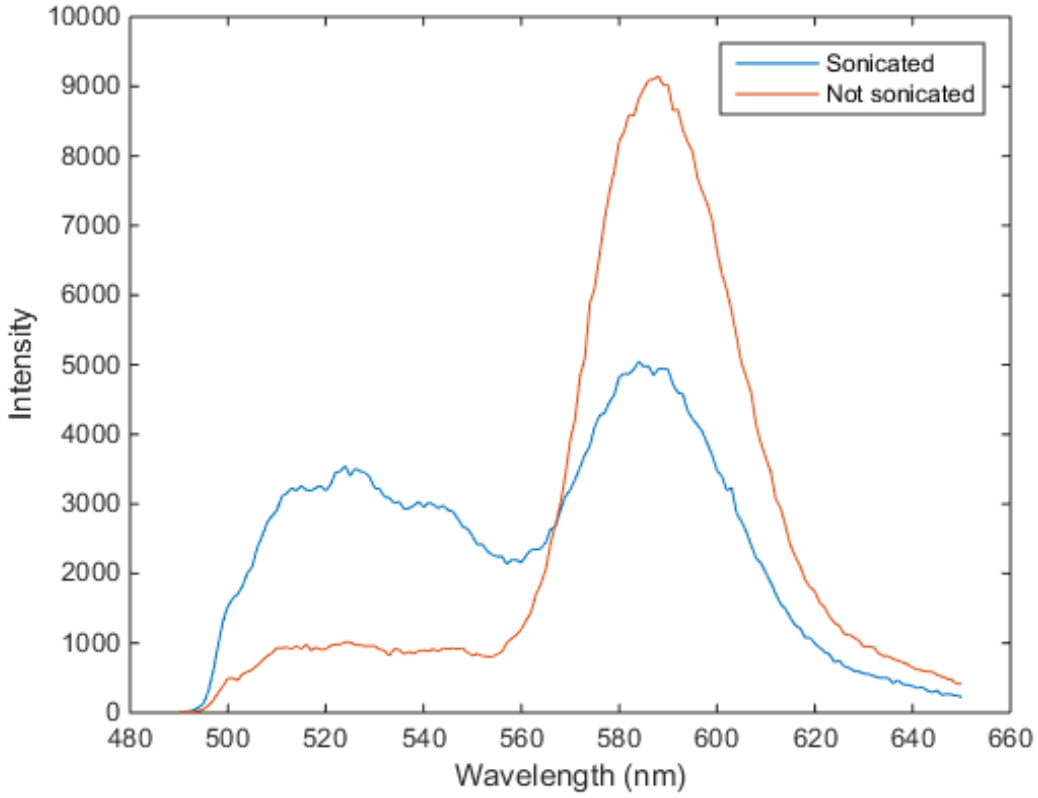

Figure 5.5: The fluorescense emission profile observed in the FRET assay. The red curve shows the emission intensity of a non-sonicated sample of NMV/FRET-vesicles in a 30:1ratio (lipid weight). The blue curve shows the corresponding intensity curve for a sonicated sample of the same composition. The sonicated sample was sonicated at 37^oC for 10 minutes.

As can be seen in figure 5.5 the emission intensity curve for the sonicated sample features two peaks, one around 530 nm, and one around 590 nm, whereas the non sonicated sample mostly displays a peak around the 590 nm mark. This is a clear indication that the NMVs mixed and fused with the FRET-vesicles since there are fewer FRET molecules able to absorb the wavelengths of 530 nm, which is most probably a result of the FRET molecules having separated during the sonication.

In order to confirm that the NMVs, once fused with PEG/POPC vesicles, could form a bilayer, TIRFM was used. Different ratios of sonicated NMV+PEG/POPC vesicles were analyzed as bilayer formation took place, the result of which can be seen in figure 5.6

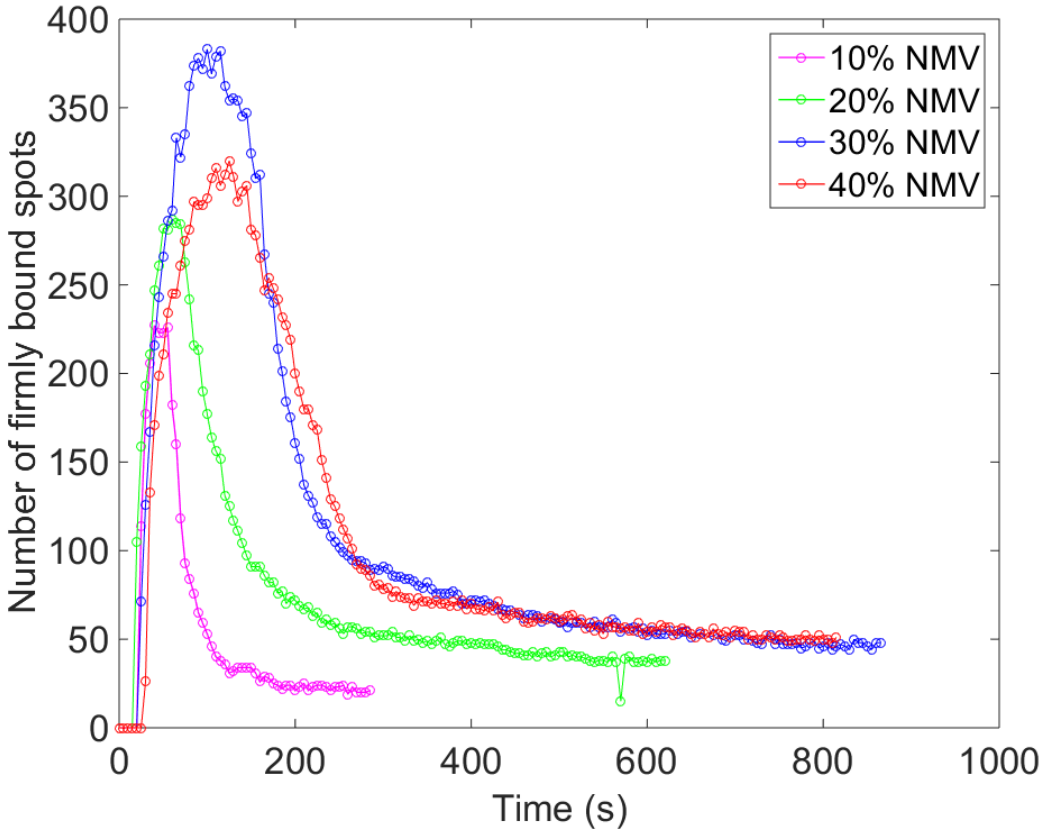

Figure 5.6: The number of unruptured vesicles containing different weight ratios of NMV+PEG/POPC as they are allowed to form bilayers in a PDMS well. Vesicles were counted on a 277,33x234 μm surface using image analysis software.

As can be seen in figure 5.6, vesicles of all ratios adhere to the surface leading to a maximum at which the number of unruptured vesicles decreases due to SLB formation. Whilst all types of vesicles managed to form a bilayer, differences can be seen as the NMV ratio increases. The figure shows that with an increased amount of NMV fraction, the time until the maximum is reached increased, as did the absolute value of the peak. This strongly indicates that vesicles containing higher amounts of NMV are less likely to form bilayers. An exception to the trend of more individual vesicles visible before bilayer formation as the ratio of NMV increases can be seen in the case of the 30% NMV vesicles. It is uncertain what causes this effect, or if the effect is just a coincidence.

5.3 Interaction with human lactoferrin

The results displayed in the previous sections strongly indicate the successful incorporation of LPS/LTA in the SLBs, and that it is possible to form bilayers containing native membranes. In order to investigate the potential of the different SLB platforms as a sensing interface, hLf was added to the different SLB in the QCM-D since hLf has been known to bind to LPS [1]. Addition of hLf did not have any significant

effect on the SLBs containing LPS-Ek and the LTA, whereas for bilayers containing LPS-Rc and for native membranes, binding was clearly obesrved as displayed in figure 5.7.

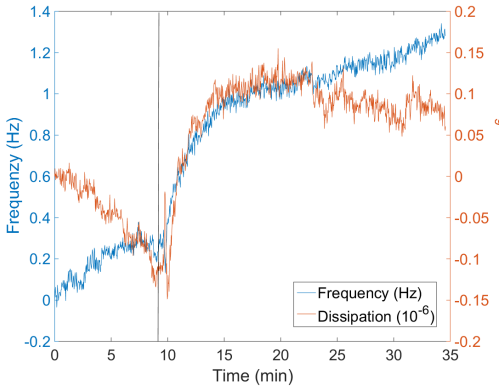

(a) The effect of hLf on a native membrane bilayer contaning 10% wt NMV and 90% wt PEG/POPC.The hLf was added at the 2 minute mark and rinsing with buffer took place at the 12 minute mark.

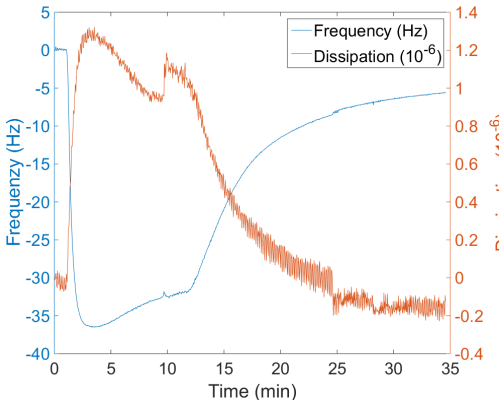

(b) The effect of hLf on a native membrane bilayer contaning 40% wt NMV and 60% PEG/POPC.The hLf was added at the 2 minute mark and rinsing with buffer took place at the 12 minute mark.

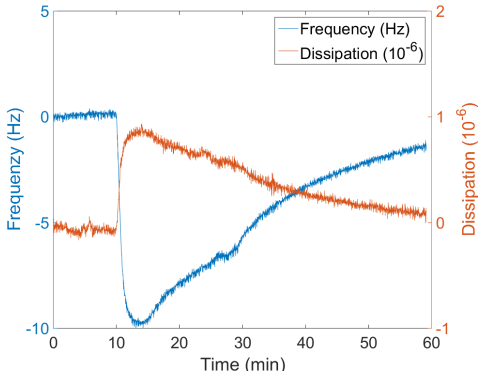

(c) The effect of hLf on a 10% wt LPS-Rc bilayer.The hLf was added at the 10 minute mark and rinsing with buffer took place at 30 minute mark.

Figure 5.7: Frequency and dissipation vs time (min) data displaying the effect of hLf flowing over a SLBs containing LPS-Rc or native membranes. Frequency and dissipation has been set to zero before hLf introduction in order to better illustrate the interactive effect.

The lack of hLf binding to the bilayers containing LTA could be due to the fact that hLfs principal target is the lipid A part at the root of the LPS [1] and LTA does not posses any lipid A part to which hLf could bind. In the case of LPS-Ek it could be that the inner and outer core acts as a steric hindrance, stopping the hLf

from reaching the lipid A part of the LPS. It could also be possible that electrical charges present on the sugars of LPS-Ek acts as a hindrance for the hLf-Lipid A interaction. LPS-Rc, on the other hand, has a much shorter outer core, making for less of a hindrance, which could promote the hLf-LPS interaction. Interestingly, the initial decrease in frequency and associated increase in dissipation is followed by a spontaneous increase in frequency and a decrease in dissipation after further addition of the hLf protein. Since hLf has been known to displace LPS in bacterial membranes it is possible that this displacement is what can be observed in figure 5.7c [1]. This same effect is visible in the native membranes in figure 5.7b indicating that the interactive mechanism between hLf and LPS is similar in the two bilayers. Figure 5.7a shows little sign of binding at all, most likely due to the fact that for this bilayer the amount of native material incorporated was too low to generate a detectable signal.
Since the hLf showed clear interaction with LPS-Rc, it was of interest to see if the interaction induced a change in the properties of the SLB. In order to investigate this, FRAP was performed on a SLB containing LPS-Rc and the diffusion coefficient and immobile fraction before and after the addition of hLf was compared. As visible in table 5.2 binding of hLf did not have any significant effect on the bilayer fluidity.

5.4 Interaction with Adenovirus type 40

In a second step, the binding of AdV40 to the different bilayers was investigated using QCM-D. Under all conditions investigated there was very little binding, exemplified by figure 5.8.

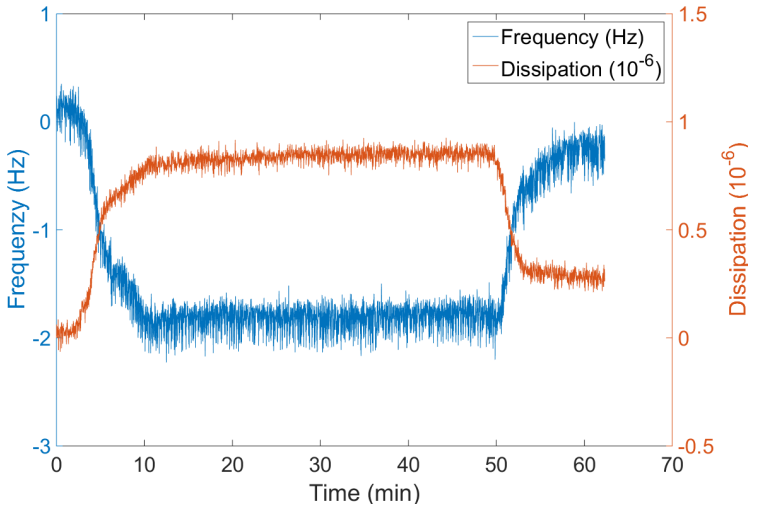

Figure 5.8: A representative illustration showcasing the QCM-D response when adding AdV40 to a bilayer containing 10%LPS-Ek, 10%LPS-Rc, or 10%LTA. The figure shows frequency and dissipation vs time (min) data for 10%LPS-Ek. The AdV40 was introduced at the 5 min mark and PBS buffer was introduced at the 50 min mark. Frequency and dissipation has been set to zero before AdV40 introduction in order to better illustrate the interactive effect.

As can be seen in figure 5.8, the introduction of AdV40 caused a frequency and dissipation change to be detected in the QCM-D. This change reverted for the most part once the AdV40 was replaced by the PBS buffer, indicating that no AdV40 binding took place and the difference detected could be due to the different buffer composition of the AdV40 solution as compared to the buffer in which the baseline was acquired. This phenomenon could be seen with the native membrane SLBs as well (data not shown). It was hypothesized that the lack of binding could be due to the possibility that the incorporated LPS-Ek molecules were too densely packed and acted as a steric hindrance for AdV40-LPS interaction. Experiments involving surface densities of LPS-Ek were thus carried out, the results of which can be seen in figure 5.9.

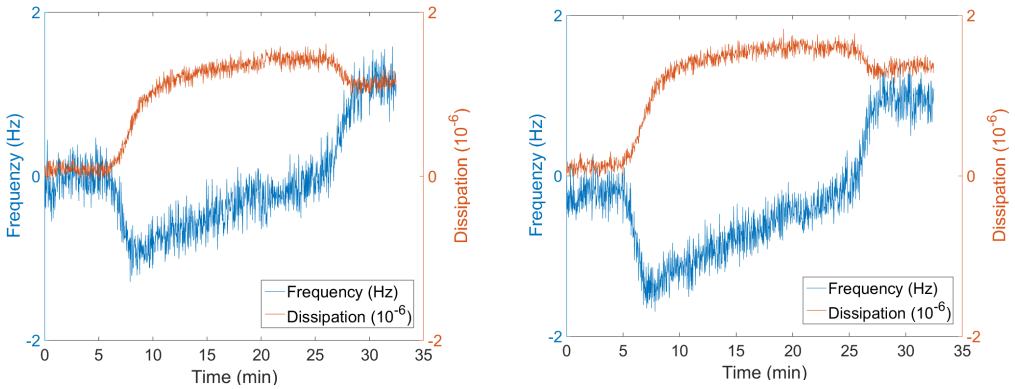

(a) Interaction between AdV40 and SLB with 0.05% wt incorporated LPS-EK.

(b) Interaction between AdV40 and SLB with 2% wt incorporated LPS-EK.

Figure 5.9: Frequency and dissipation vs time (min) data for 0.05 and 2 %LPS-Ek. The AdV40 was introduced around the 5 min mark and PBS buffer was introduced around the 27 min mark. Frequency and dissipation has been set to zero before AdV40 introduction in order to better illustrate the interactive effect.

As can be seen in figure 5.9, addition of AdV40 viruses to SLBs of lower LPS content leads to a slight adsorption of viruses, mainly visible in the dissipation signals which remain elevated after the introduction of buffer to the system. It is possible that the LPS-Ek indeed acted as a steric hindrance for the interaction. The trends seen in these results are, however, very slight and the reason for this is most likely that almost no AdV40-LPS-Ek interaction takes place.
To investigate the interaction with higher sensitivity, the AdV40-LPS interaction was also studied using TIRFM, which allows for the visualization of LPS-virus interaction on a single particle basis. In the setup, two sets of bilayers were created using vesicles containing 2% and 0.05% LPS-Ek by weight. AdV40 solution was added on top of the bilayers and fluorescent vesicles with the same LPS composition as the bilayers were added on top of the virus in order to visualize the interaction. The results can be seen in figure 5.10.

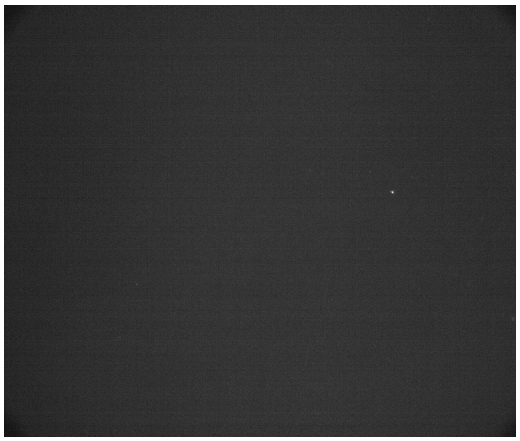

(a) Bilayer containing 2% LPS-Ek by weight with fluorescent vesicles added without being subjected to AdV40 (negative control). Two or three vesicles are visible.

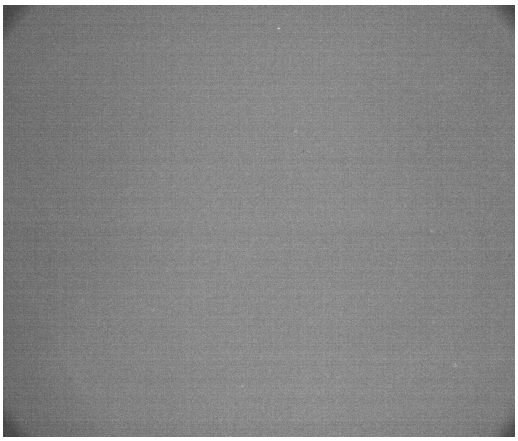

(b) Bilayer containing 2% LPS-Ek by weight with fluorescent vesicles added to the bilayer after being subjected to AdV40. Less than ten vesicles could be spotted.

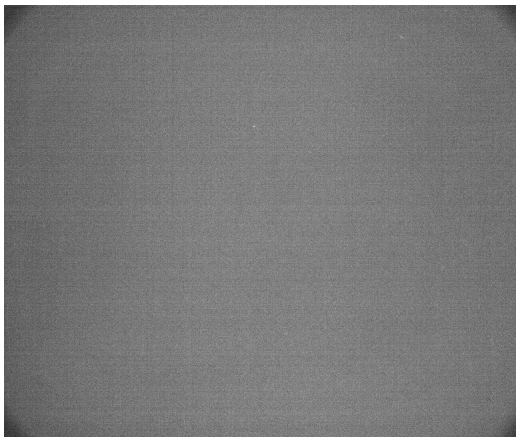

(c) Bilayer containing 0.05% LPS-Ek by weight with fluorescent vesicles added without being subjected to AdV40 (negative control). Less than ten vesicles could be spotted.

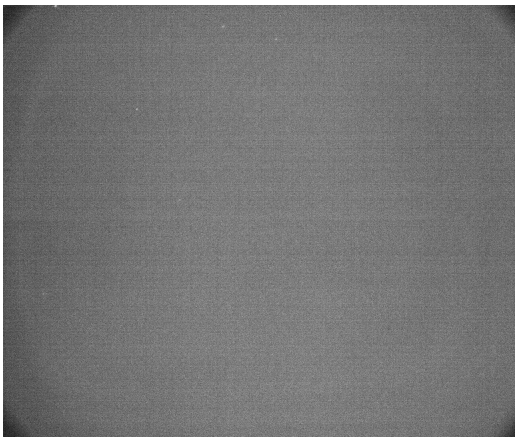

(d) Bilayer containing 0.05% LPS-Ek by weight with fluorescent vesicles added to the bilayer after being subjected to AdV40. Less than ten vesicles could be spotted.

Figure 5.10: TIRFM results of interaction probing between AdV40 and LPS-Ek - containing bilayers of different compositions. Fluorescently marked vesicles were introduced to wells containing the bilayers and AdV40, (b) and (d), and the vesicles were also introduced to wells containing just bilayers, (a) and (c).

As can be seen when comparing figures 5.10a and 5.10b, as well as figures 5.10c and 5.10d, there is really no difference between them. The results show that no significant binding of the fluorescent vesicles could be detected, neither to the negative control, nor to the bilayers in the wells containing virus. This further supports the claim that AdV40 does not adhere to bilayers containing LPS-Ek.

6
Discussion

Two types of sensing platforms have been investigated during the course of this project, the NMV-bilayers and the bilayers constructed from synthetic vesicles containing LPS. Depending on the envisioned application it might be more favorable to use one of the bilayer types rather than the other one, since both have their advantages and disadvantages.
The native-SLB platform holds great promise as a platform for biomolecular sensing in the context of probing biomolecular interactions in a comprehensive manner, i.e. by having all bacterial molecules present at the sensing interface. However, a setback is the fact that when dealing with native membrane surfaces it can be difficult to determine which molecule is involved in an interaction and whether the interaction is mediated by two or more biomolecular binding partners. Considering this, the combination of an experimental approach based on a minimal model system created following a bottom up approach and containing one or a few components with a top-down approach based on the NMVs could be useful in order to determine if a surface-molecule interaction is dependent on several membrane molecules, or just one. This promises to create a better understanding regarding the importance and mode of action of supporting binding partners in surface-molecule interactions.
In this thesis, we have further used the different SLB platforms to investigate binding of biological entities. At first, the binding of hLf to LPS was investigated, and binding to LPS-Rc containing bilayers and native membranes was confirmed although it exhibited a non-conventional binding behaviour (figure 5.7). From the observed signal it was hypothesised that additional binding of the hLf leads to a partial displacement of the LPS in agreement with current literature [1]. However, a displacement of the incorporated LPS in the SLB is probable to cause damages to the SLB as a whole, making it porous and loose. A porous and loose membrane would probably change the overall viscoelastic properties of the surface, and possibly allow for a greater amount of water to be coupled to it, which in turn might result in a higher dissipation response and a lower frequency response in comparison with figure 5.7. Another hypothesis possibly explaining the observed results is that hLf simply dissociates again upon reaching a critical surface coverage and hence exhibits a so-called overshoot behaviour. Further analysis using surface sensitive techniques could perhaps be performed in order to confirm this hypothesis, such as maybe liquid-based AFM or perhaps SPR, since both could provide a better insight as to how the hLf is positioned on the bilayer surface.
Another interaction that was investigated in this project was the interaction between LPS-Ek containing SLBs and Adenovirus type 40, performed in order to see if LPS could have any sort of stabilizing effect on AdV40. The results obtained showed little

to no interaction taking place with either type of bilayer, neither the ones derived from synthetic vesicles, nor the ones derived from NMVs. This observation is in disagreement with the observation of our collaborators from Niklas Arnbergs group in Umeås university who have, using dot blotting, confirmed the AdV40 LPS-Ek interaction, albeit in this case the LPS was added in solution and was not membrane bound. A possible explanation reconciling both observations is that the virus binds to secreted LPS (i.e. in solution but not to membrane bound ones) and that the LPS, when bound to a surface, can't access the viral proteins involved in the interaction due to steric hindrance in order for it to bind properly. This could be the case, if for example, the site of binding on the virus is located on the surface capsid of the virus, as opposed to on the glycoproteins protruding from the surface. looking at figure 2.1, it does look possible that the glycoproteins acts as the steric hindrance, keeping the LPS from interacting with the surface capsid. The binding to less exposed capsid proteins rather than to the protruding glycoproteins has, for example, been reported in the case of other viruses, in particular the poliovirus as shown by Christopher M. Robinson et al [6]. This study looks at the effect of LPS on the poliovirus, another enteric virus. The study confirms virus-LPS interaction and also suggests a binding site for the LPS to the poliovirus on the surface capsid of the virus itself. If this is the case, then perhaps a better approach to study adenovirus 40 - LPS interaction might be to firmly attach the virus to a surface (for example a QCM-D crystal), and then introduce free LPS in solution to the flow. This approach could show if the free LPS bind to the virus capsid, and if this binding is confirmed, then this approach could also be used to study the stability of the capsid. This could be done by comparing the dissipation and frequency responses over time between LPS-subjected virus and virus not subjected to LPS.
It cannot, however, be excluded that there are other problems with the virus-surface interactions that does not have anything to do with steric hindrance. It is also possible that the quality of the virus once introduced to the bilayers in our lab is such that it does not perform properly. Maybe the virus falls apart and the small amount of virus that does remain intact is not enough for the instruments to register. Potential monomers present in the virus solution might also remain undetected. It is, for example, possible that the monomers bind to the LPS in the bilayer in a way such that they do not contribute to the coupling of water in the QCM-D and thus does not significantly alter the frequency and dissipation response upon binding.

7
Conclusion

The results obtained during the course of this project indicate that it is indeed possible to integrate LPS/LTA in POPC vesicles and have them form bilayers. It is also confirmed that bilayer formation is possible using vesicles containing native membranes extracted from bacteria. The created SLBs were able to interact with some types of biomolecules, indicating that SLBs of different types could be a useful tool when investigating different cell surface specific interactions. The study of said interactions could, for example, facilitate the development of more sophisticated drugs, by acting as a platform to study their binding but also to investigate how they act on the membrane.

Bibliography

[1] Jesús S. Luna Rafael Campos-Rodríguez Maria E. Drago-Serrano, Mireya de la Garza-Amaya. Lactoferrin-lipopolysaccharide (lps) binding as key to antibacterial and antiendotoxic effects. *International Immunopharmacology*, 12:1–9, 2011.

[2] Chris A. Etheredge Andrea J. Pruijssers Johnna M. Frierson Lora V. Hooper Terence S. Dermody Julie K.Pfeiffer. Sharon K. Kuss, Gavin T. Best. Intestinal microbiota promote enteric virus replication and systemic pathogenesis. *Science*, 14:249–252, 2011.

[3] Adenovirus (serotypes 40 & 41) pathogen safety data sheet - infectious substances. `http://www.phac-aspc.gc.ca/lab-bio/res/psds-ftss/adenovirus-eng.php`.

[4] Alireza Mashaghi Marcus Textor Bernard Priem Markus Aebi Erik Reimhult Stefan Kaufmann, Karin Ilg. Supported lipopolysaccharide bilayers. *Langmuir*, 28:12199–12208, 2012.

[5] Arwel V Hughes Emma L Daulton Wanatchaporn Arunmanee Frank Heinrich Syma Khalid Damien Jefferies Timothy R Charlton John R P Webster Christian J Kinane Luke A Clifton, Stephen A Holt and Jeremy H Lakey. An accurate in vitro model of the e. coli envelope. *Angew Chem Int Ed Engl*, 54:11952–11955., 2015.

[6] Palmy R. Jesudhasan Christopher M. Robinson and Julie K. Pfeiffer. Bacterial lipopolysaccharide binding enhances virion stability and promotes environmental fitness of an enteric virus. *Cell Host & Microbe*, 15:36–46, 2014.

[7] Molecule of the month. `http://pdb101.rcsb.org/motm/132`.

[8] Glen Burnie. Quartz crystal microbalance: A useful tool for studying thin polymer films and complex biomolecular systems at the solution - surface interface. *Journal of Biomolecular Techniques*, 322(19):151–158, 2008.

[9] Jiri Janata. *Principles of Chemical Sensors*. Springer Science & Business Media, 2013.

[10] Erik Nilebäck. *QCM-D With focus on biosensing in biomolecular and cellular systems*. PhD thesis, Chalmers University of Technology, 2013.

[11] Claes Nylander Bo Liedberg and Ingemar Lundström. Surface plasmon resonance for gas detection and biosensing. *Sensors and actuators*, 4:299–304, 1983.

[12] Daniel Axelrod. Total internal re¯ection fluorescence microscopy in cell biology. *Munksgaard International Publishers*, 2:764–774, 2001.

[13] Research: Total internal reflection fluorescence microscopy (tirf). https://www.dkfz.de/Macromol/research/tirf.html.

[14] Richard Ankerhold Hellen C. Ishikawa-Ankerhold and Gregor P. C. Drummen. Advanced fluorescence microscopy techniques - frap,flip, flap, fret and flim. *Molecules*, 17:4047–4132, 2012.

[15] Anne K. Kenworthy Minchul Kang, Charles A. Day and Emmanuele DiBenedetto. Simplified equation to extract diffusion coefficients from confocal frap data. *Traffic*, 13:1589–1600, 2012.

[16] Jonas O. Tegenfeldt Peter Jönsson, Magnus P. Jonsson and Fredrick Höök. A method improving accuracy of fluorescence recovery after photobleaching analysis. *Biophysical Journal*, 95:5334–5348, 2008.

[17] Fluorescence resonance energy transfer (fret) microscopy. `http://www.olympusmicro.com/primer/techniques/fluorescence/fret/fretintro.html`.

[18] Roger Michel Marcus Textor Ilya Reviakine Fernanda F. Rossetti, Marta Bally. Interactions between titanium dioxide and phosphatidyl serine-containing liposomes: Formation and patterning of supported phospholipid bilayers on the surface of a medically relevant materialy. *Langmuir*, 21:6443–6450, 2005.

[19] Gustav Emilsson Virginia Claudio Stephan Block Cecilia Lässer Andreas Dahlin Jan O. Lötvall Marta Bally Vladimir P. Zhdanov Déborah L. M. Rupert, Ganesh Vilas Shelke and Fredrik Höök. Dual-wavelength surface plasmon resonance for determining the size and concentration of sub-populations of extracellular vesicles. *Not yet published*, Not yet published:30, Not yet published.

A

Appendix 1

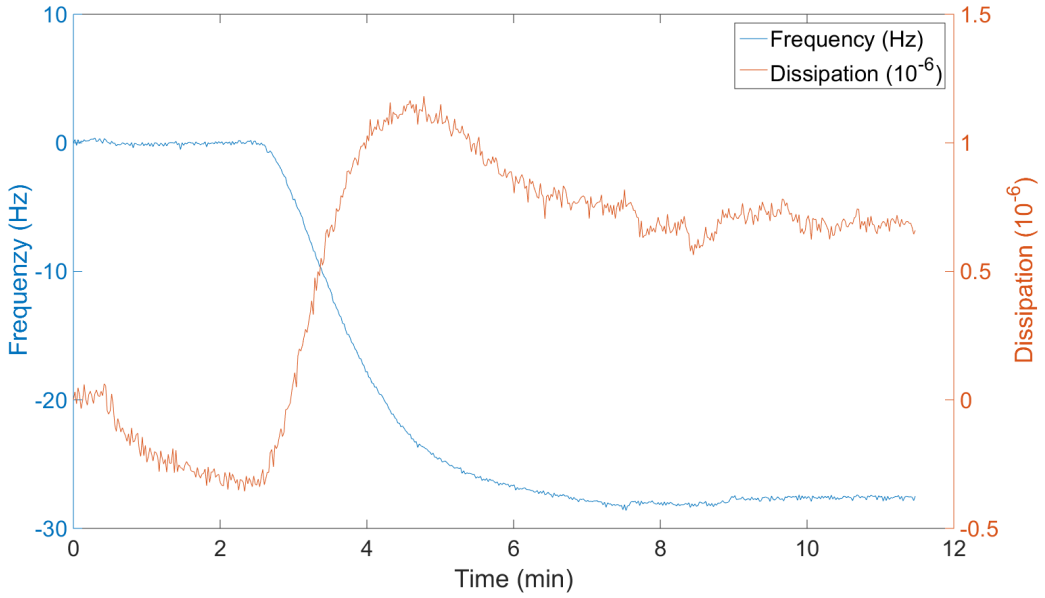

(a) Bilayer formation with 10% LPS-Ek containing vesicles using low pH buffer (pH 4.8).

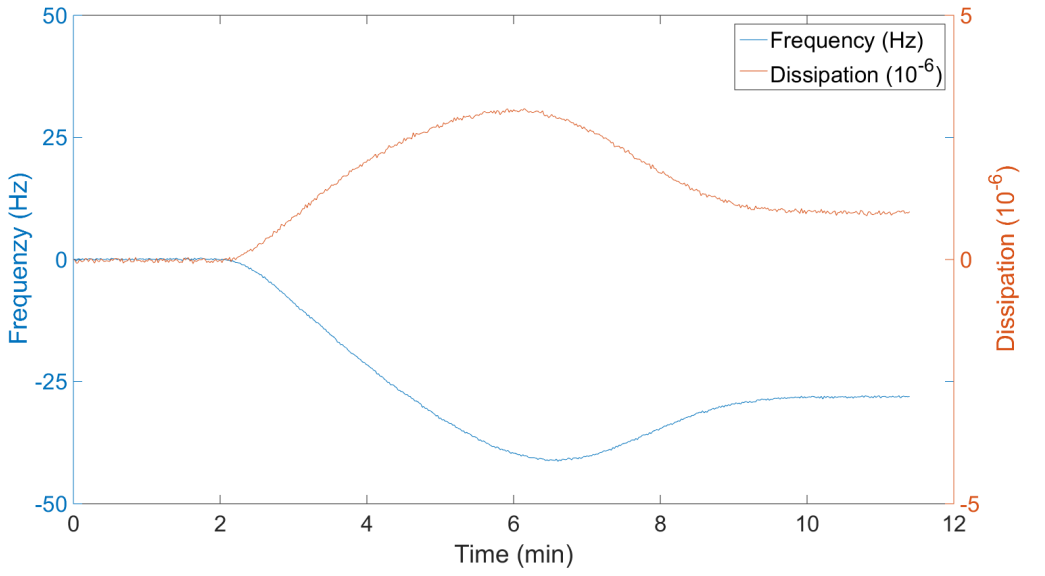

(b) Bilayer formation with 10% LPS-Ek containing vesicles using calcium buffer.

Figure A.1: Bilayer formation with 10% LPS-Ek containing vesicles using two different buffers.

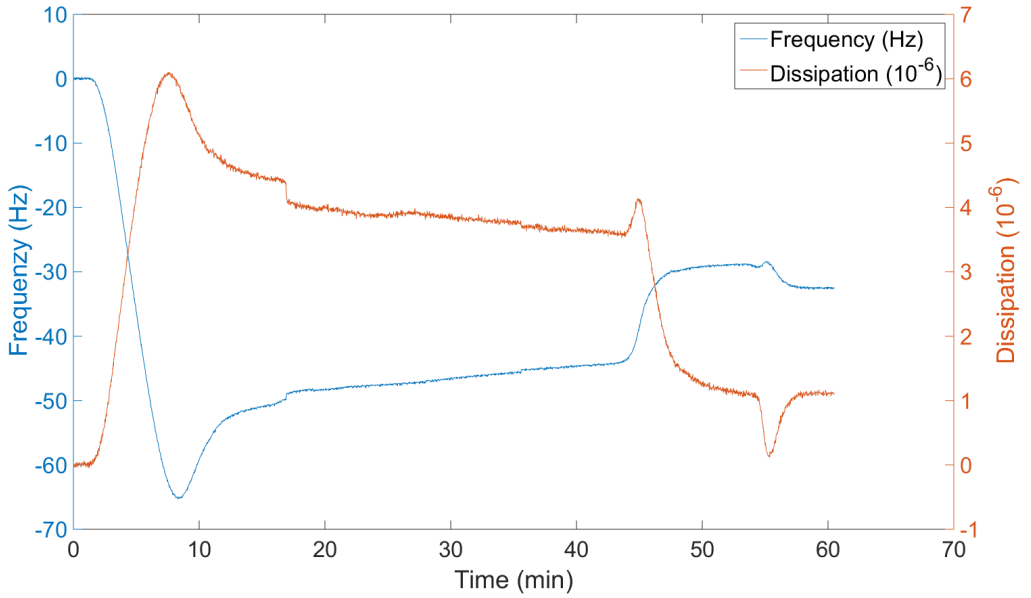

(a) Bilayer formation with 10% LPS-Rc containing vesicles using low pH buffer (pH 4.8).

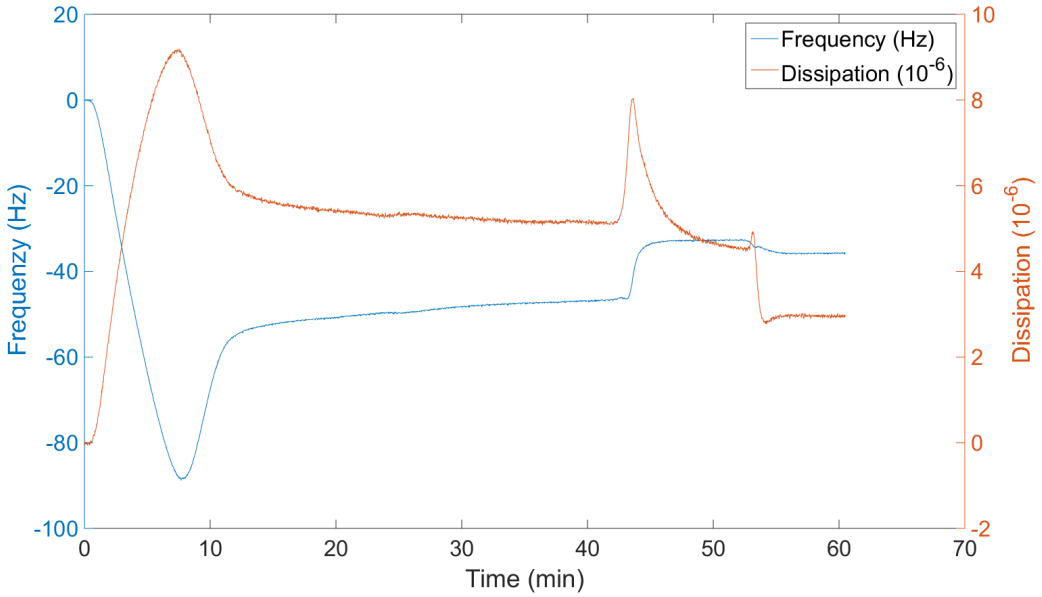

(b) Bilayer formation with 10% LPS-Rc containing vesicles using calcium buffer.

Figure A.2: Bilayer formation using 10% LPS-Rc containing vesicles using two different buffers. A 10 min osmotic shock is performed around the 45 min mark. The small dent seen in the dissipation in (a) around 55 min is probably an artefact caused by the introduction of buffer after osmotic shock.